

Three-dimensional structure of the basketweave Z-band in midshipman fish sonic muscle:
implications for α -actinin and actin binding

Thomas Burgoyne^{1,8*}, John Heumann^{2*}, Edward Morris^{3*}, Carlo Knupp^{4*}, Jun Liu^{5,9}, Mike Reedy⁶,
Kenneth A. Taylor⁵, Kuan Wang⁷, Pradeep K. Luther^{1#}

1 Molecular Medicine Section, NHLI, Imperial College London, London SW7 2AZ, UK

2 Boulder Laboratory for 3D Electron Microscopy of Cells, Department of Molecular, Cellular and
Developmental Biology, University of Colorado, Boulder, CO 80309-0347, United States.

3 Institute of Cancer Research, London SW7 3RP, UK.

4 School of Optometry and Vision Sciences, Cardiff University, Cardiff, CF10 3AT, UK.

5 Institute of Molecular Biophysics, Florida State University, Tallahassee, FL 32306-4380

6 Department of Cell Biology, Duke University Medical Center, Durham, NC 27710, United States.

7 Laboratory of Muscle Biology, NIAMS, NIH, Bethesda, MD, United States and College of Biomedical
Engineering, Taipei Medical University, 250 Wuxing Street, Taipei 11031, Taiwan.

8 Current Address: UCL institute of Ophthalmology, London, EC1V 9EL.

9 Current Address: Dept. of Microbial Pathogenesis, Yale School of Medicine, 333 Cedar Street, New
Haven, CT 06510

* These authors contributed equally

Corresponding author

Pradeep K Luther

Molecular Medicine Section

National Heart and Lung Institute

Imperial College London

London SW7 2AZ

Email: p.luther@imperial.ac.uk

Tel: +44 7766766212

Classification: Biophysics and Computational Biology

Abstract

Striated muscle enables movement in all animals by the contraction of myriads of sarcomeres joined end to end by the Z-bands. The contraction is due to tension generated in each sarcomere between overlapping arrays of actin and myosin filaments. At the Z-band, actin filaments from adjoining sarcomeres overlap and are crosslinked in a regular pattern mainly by the protein α -actinin. The Z-band is dynamic, reflected by the two regular patterns seen in transverse section electron micrographs; the so-called small-square and basketweave forms. Although these forms are attributed respectively to relaxed and actively contracting muscles, the basketweave form occurs in certain relaxed muscles as in the muscle studied here. We used electron tomography and subtomogram averaging to derive the three-dimensional structure of the Z-band in the swimbladder muscle of male Type 1 Plainfin midshipman fish (*Porichthys notatus*), into which we docked the crystallographic structures of actin and α -actinin. The α -actinin links run diagonally between connected pairs of anti-parallel actin filaments and are oriented at an angle of about 25° away from the actin filament axes. The slightly curved and flattened structure of the α -actinin rod has a distinct fit into the map. The Z-band model provides a detailed understanding of the role of α -actinin in transmitting tension between actin filaments in adjoining sarcomeres.

213 words (limit 250)

Keywords

Z-line, Z-disc, α -actinin, actin, electron tomography, subtomogram averaging

Significance Statement

Striated muscle enables movement in all animals by the contraction of myriads of sarcomeres joined end to end by the Z-bands. The contraction is due to tension generated in each sarcomere between overlapping arrays of actin and myosin filaments. At the Z-band, actin filaments from adjoining sarcomeres overlap and are crosslinked mainly by the protein α -actinin. In this study, we used electron tomography and subtomogram averaging to derive the three-dimensional structure of the Z-band in swimbladder muscle of Plainfin midshipman fish, into which we docked the atomic coordinates of actin and α -actinin. The Z-band model provides a detailed understanding of the role of α -actinin in transmitting tension between actin filaments in adjoining sarcomeres.

109 words (limit 120)

Introduction

Striated muscles are agglomerates of myriads of sarcomeres joined end to end by the Z-bands (Z-lines, Z-discs) and contraction of muscle occurs when sarcomeres shorten. Each sarcomere comprises two inwardly facing arrays of actin filaments which are attached at the Z-band at one end and overlap at the other end with the centrally located array of myosin filaments (1). Sarcomere shortening is due to the actin filaments moving past the myosin filaments towards the centre of the sarcomere. The barbed ends of actin filament of adjoining sarcomeres overlap in the Z-band and are crosslinked in precise patterns mainly by the rod-shaped protein α -actinin.

The Z-band in vertebrate striated muscle is dynamic and in cross-sectional view manifests two patterns, the so-called basketweave and small-square lattice forms (1-3). In this study we examine the structure of the basketweave Z-band of a specialised muscle in the relaxed state. However the two forms are generally thought to result from the contractile state of the muscle, the basketweave attributed to contracting muscle while the small-square form is attributed to relaxed muscle. As there is a physical change in the Z-band during contraction, it may have a role in mechanotransduction. It is thought that the small-square form is due to sharply bent Z-band links whereas the basketweave form is due to straightening of the links and a small lattice expansion as could occur during contraction (2, 3). However the molecular nature of this transformation is not known. We note that the basketweave form in relaxed muscle has been seen in other species: fish fin muscle (4) and bovine neck muscle (5). It is not known what form the Z-bands of these muscles adopt during contraction. Some researchers have proposed that the Z-band state may be due to the movement of tropomyosin on actin (2).

In longitudinal view, the Z-band presents as a dense band defining sarcomere boundaries. The Z-band has a characteristic width which depends on the muscle type: it is narrowest in fast muscles (~60-100 nm) and wider in slow and cardiac muscles (100-140 nm)(6). The Z-band is the location of a multitude of proteins with various functions, and mutations in these proteins lead to skeletal and cardiac disease (7). Understanding the fine structure of the Z-band will clearly help us to understand the role of the Z-band in health and disease.

The variation in Z-band width between different muscle types noted above arises from the extent of overlap between the actin filaments from adjacent sarcomeres and the number of layers of the zig-zag structure arising from the connecting links between actin filaments (6). The primary component of these connecting links in the Z-band is α -actinin, a member of the spectrin family. α -

actinin is a ubiquitous protein in the eukaryote cytoskeleton (8-10); it is a homodimer of length 360 Å whose crystal structure was solved recently (11). It is composed of two antiparallel rod-shaped monomers. Each monomer is composed of an N-terminal actin binding domain (ABD) consisting of two calponin homology domains (CH1 and CH2), a rod domain comprising 4 spectrin domains, and a C-terminal region comprising two pairs of EF hand domains, EF1-2 and EF3-4 (11). While the ABD is flexible and can bind actin in a variety of conformations (12), the rod domain is rigid with a small curve (11, 13).

To understand the Z-band dynamic states exhibiting small-square and basketweave conformations, we need to determine the structures of these states at a resolution sufficient for docking the atomic models of actin and α -actinin. Ideally, the sample should be homogeneous in morphology. It is fortuitous that the structure of the sarcomere in all vertebrate striated muscle, including skeletal and cardiac, is very similar, which gives us the freedom to select the most favourable sample for a particular study(14). The muscle surrounding the swim bladder of male Type 1 Plainfin midshipman fish (*Porichthys notatus*) provides a favourable sample of the basketweave Z-band form. Whereas normal Z-bands have narrow axial widths ranging from 60 to 140 nm discussed above, this so-called sonic muscle has a highly specialised Z-band which is exceptionally wide $\sim 1.2 \mu\text{m}$ (Fig 1a) and highly ordered (Fig 1b-d): its unusual width arises from multiple layers of the underlying α -actinin linkage (15). The multiple layers contribute to the high level of order of the sonic Z-band as well as greatly increasing the number of individual repeating structures available for averaging. These factors make the sonic Z-band particularly favourable for structure determination by electron microscopy. Apart from the unusual width of the Z-band, the A-bands and sarcomeres of the sonic muscle are normal, although the myofibrils are significantly narrower than other muscle types ($\sim 0.2 \mu\text{m}$). *P. notatus* are normally deep sea fish which emerge into coastal regions during the mating season and make low frequency ($\sim 100\text{Hz}$) humming sounds with these sonic muscles (16).

In this study we have elucidated the 3D structure of the Z-band in the basketweave form in the sonic muscle of midshipman fish by electron tomography and subtomogram averaging. Our reconstruction has enabled us to fit the crystallographic structures of α -actinin and actin into the map, solving one of the two main conformational states of the vertebrate Z-band and giving a detailed understanding of the role of the Z-band in transmitting tension between actin filaments in adjoining sarcomeres.

Results

For this study, we used 100 nm thick transverse sections of resin-embedded sonic muscle Z-band. The muscle was treated in 50 mM butanedione-monoxime, an inhibitor of skeletal muscle myosin (17) thereby ensuring that the muscle is in a relaxed state. Electron microscopy of transverse sections showed a clear homogeneous basketweave form (Fig 1d and Fig S1a). Although we collected tomograms of both transverse and longitudinal sections for this study, the former were found to be much more informative and are described here. The results of the latter are briefly described later. Tomograms were calculated from tilt series of sections of the sonic muscle Z-band as described in materials and methods. An image of the projected tomogram is shown in Fig S1a; it comprises two myofibrils in cross-section. A movie paging through the depth of the tomogram is shown in Movie S1. As the sonic muscle Z-band is a 3D crystal, the movie shows recurring basketweave motifs through the depth of the tomogram.

Scrutiny of the Z-band in Figs 1d and S1a shows that the Z-band is based on an approximate tetragonal lattice but the lattice is not coherent over the whole myofibril. The lattice is regular over small clusters ~ 0.5 to $1 \mu\text{m}$ in size like the example outlined in Fig S1a. Viewing the image at a glancing angle accentuates the boundaries between the ordered clusters and shows up the dislocations between them. To obtain a mean 3D image of the Z-band various methods can be used. As these clusters are quite small, crystallographic tilt reconstruction (18, 19) cannot be used. We decided to use subtomogram averaging using as our subvolume (or particle) the Z-band region as outlined with a dashed box in the upper part of the Z-band in Fig 1e.

To enable accurate subtomogram averaging and symmetrisation over subvolumes with varying orientations, it is essential that the sample not be distorted. Thin sections of plastic embedded samples as used in this study are typically compressed during ultramicrotomy. Our correction of the compression is discussed in Supplementary Information. Such sections also experience shrinkage during the preparation and during the electron microscopy (20). Our scaling for the dimensional changes is also discussed in Supplementary Information.

Z-band subvolumes within the tomogram were extracted from the Z-band areas in the tomogram (Fig S1d) and averaged using the subtomogram averaging program PEET (21, 22). Semi-automated particle picking was performed by iterative refinement starting from a manually chosen

single-particle initial reference and a uniform, 2D grid of initial locations with spacing approximating that of the unit cell. Selected points were windowed via cross-correlation thresholding and manual editing before further alignment and averaging, giving 483 points.

The basis for the subtomogram averaging was as follows. An actin filament is composed of a helix of actin monomers as shown schematically in Fig 1f with coloured spheres representing actin monomers. Adjacent red and blue spheres each with a short stub (referred to here as a *symmetry pair*) highlight symmetry related points along the filament which are relevant for Z-band assembly. We assumed symmetry for actin comprising 28 subunits in 13 turns of the short pitch helix (28/13, also called genetic helix) as found previously in insect flight muscle (23), nemaline rod (24) and skeletal muscle Z-bands (25), which connects every actin subunit, giving a 167.1° rotation per subunit. Combined with an axial rise per subunit of 27.4 \AA (Egelman et al., 1982), after 7 subunits we have net rotation of 90° i.e. a $\frac{1}{4}$ turn and an axial displacement of 192 \AA . The full axial repeat of the system comprises 28 subunits spanning 768 \AA . A special feature of a symmetry pair is that the two links on either side of a filament have a relative 27.4 \AA offset, giving a distinct asymmetric appearance. While visible in our subtomogram averages, this offset is a weak feature at the resolution achieved. In addition the 167.1° rotation is close to 180° , which tends to give the illusion of 2-fold rotational symmetry. Subtomogram averaging was applied at the subvolume coordinate as well as $\pm 192 \text{ \AA}$ translation along the filament accompanied respectively with $\pm 90^\circ$ rotation. Two C2 axes orthogonal to the filament axis were identified with relative axial shifts of $\pm 192 \text{ \AA}$ (shown by arrow in Fig 3a). Starting from the 483 particles, these symmetry operations provided 5796 asymmetric units for subtomogram averaging. Additional symmetries are expected and present, but their use for subtomogram averaging was precluded by the chosen subvolume size and the limited z height included in the tomogram, e.g. see Fig S3b. The resolution of the average was estimated by a Fourier Shell Correlation plot (Fig S2) which gave a value of 39 \AA for a cut-off of 0.5. This is a good value for a plastic embedded sample. Note that despite the FSC giving a value that would predict the visibility of actin subunits, no actin subunits are resolved in either the raw tomograms or the subtomogram averages. This could mean that the actin filaments are insufficiently preserved to retain visibility of the actin subunits in the tissue blocks or the sections, or it may be due to the unfavourable orientation of the filaments for viewing the F-actin subunits in the transverse sections.

The Z-band average was computationally cloned back into the original tomogram; three projection images are shown in Fig S3 and a walk-through of the stack is shown in Movie S2. The cross-sectional image, Fig S3a, replicates features of the raw tomogram projection (Fig S1d) in a

noise reduced form. Figs S3(b) and (c) show thin and thick, edge-on projections along the black line in Fig S3(a). Fig S3(b) shows that there are about three half-repeats of 380 Å in the depth of the tomogram, while (c) shows a typical chevron appearance of the Z-band comparable with a regular electron microscope image of the basketweave Z-bands in sonic muscle (Fig 1b).

The three-dimensional structure of the Z-band and docking of actin and α -actinin

We describe the results of the subtomogram averaging of the basketweave Z-band in Figs 2, 3 and in Movie S3. Fig 2 is composed of 3 columns (1-3). The region displayed comprises about one unit-cell in cross-section with two actins of one orientation and two of the opposite orientation. The axes are shown in all the panels, colour coded red, green and blue for x, y and z axes respectively. Column 1 shows surface rendered views of the subtomogram average, (a) as a transverse view and (d,g,j) as longitudinal views showing (d) (11) view, (g) (10) view and (j) (01) view. The transverse view in Fig 2a shows very clear basketweave motif. In the longitudinal views the striking feature of the reconstruction are vertical posts with arrowheads, the actin filaments crosslinked with great regularity by diagonal struts that are α -actinin. The links are slab-like with a flattened cross-section; the narrow side is observed in the transverse view (a) and the wider side is seen in the longitudinal (11) view in (d). The actin filaments appear smooth at the resolution of the current analysis and individual monomers are not readily apparent.

For the fitting of actin and α -actinin into the 3D map (Fig 2, Column 2), we have used the 16 Å cryo-EM reconstruction of actin filament labelled with the ABD of α -actinin (PDB ID code 3LUE) (26). We first constructed an atomic model of actin with 28/13 symmetry based on the Holmes actin filament model (27). Then using Pymol we added to this model the α -actinin ABD of Galkin et al at the Z-band relevant symmetry positions (Fig. 1f). The actin-ABD composite can be seen more clearly in the right column of Fig 2 with the ABD shown in red. For α -actinin fitting, we first isolated the rod domain by deleting the ABD and EF hands at residues 247 and 784 for both monomers of α -actinin. Column 2 of Fig 2 shows the result of fitting into a semi-transparent version of the map the actin-ABD and α -actinin rod. Actin filament coordinates of one orientation are coloured green and the opposite orientation coloured yellow; the arrows on the actins in Figs 2j and l points towards the M-band. The ABD, coloured red, is the dominant feature of the actin filaments in the map. The actin-ABD composite greatly helped in docking into the map. The transverse view (b) is dominated by the curved Z-band links into which the curved rods fit nicely. As shown in Fig 1g & h, the rod atomic structure comprises a slab-like profile, which docks nicely into the slab-like profile of the links. In the

longitudinal views, for clarity, only two pairs of rods coloured blue and purple are docked into the map. The fit of these features is excellent at this resolution.

In column 3 of Fig 2 we examine the atomic coordinates in the absence of the map to see the underlying structure. The transverse view (c) clearly shows the origin of the basketweave motif. The ABDs along each actin filament line up in projection showing four prominent densities (red). In the square formed by the 4 actin filaments, two of one polarity (e.g. yellow) and two of the opposite (green), the ABDs are located either closer to the centre of the square and linked by purple rods, or further out and linked by blue rods. This rectangular shape with inward and outward curved edges gives rise to the basketweave motif. The (11) view (Fig 2f) shows why the (11) view in the electron micrographs comprises dense bands (Fig 1c) in contrast to the (10) view (Fig 1b). The reason appears to be that the ABDs and some rods (blue) line up the sides of the actin filaments enhancing the density to give the dense bands. The (10) view (Fig 2i) shows the origin of the chevron motif. The motif arises due to the projection of two sets of linking rods at different but adjacent levels e.g. blue and purple, giving an apparent periodicity of 384Å. This effect is not apparent in the (01) view (Fig 3l) as the relevant linking rods have not been drawn.

The molecular structure of the sonic muscle basketweave Z-band is examined in further detail in the stereo views in Fig 3. The rods in this figure are enclosed in slabs of size 242x49x31 Å (13) in order to highlight the orientation of the rods. Fig 3a depicts a transverse view enclosing a depth of about 25nm which includes only one complete α -actinin (2 ABDs plus the purple rod). The thin edge (31 Å) of the slab is viewed end-on. Rotating the view by 90° along the X-axis gives the (11) longitudinal view in (b) cropped to include only one diagonal rod layer. The angled purple rod is now enclosed in the wide face (49 Å) of the slab as expected from the 90° rotation. As α -actinin is located in the (11) plane, we can measure the angle it subtends to actin which is 25°. Previous studies have shown that α -actinin can attach to actin in various orientations (12). Here we note that the ABD roughly follows the path of the rod and there is no major bend.

Modelling the mechanics of the Z-band

From the results of this study, we can start to investigate how tension generated in each sarcomere during contraction is handled in the Z-band. We constructed a simple model comprising two sets of actin filaments from adjoining sarcomeres on an interdigitating 262 Å square lattice extending over a circular area about 0.5 μ m in diameter (Fig S4 a and b show a longitudinal and a transverse section respectively). α -actinin was represented by thin cylinders of length 360 Å (full

length of α -actinin including the ABD) connecting the actin filaments at the ABD attachment positions. The anti-parallel actins were linked with four layers of α -actinin; each adjacent layer being separated by 192Å and with a relative rotation of 90°. The actins along the circumference of the model were immobilised to simulate the sarcolemma and extra-cellular matrix, however the spatial extent of the model is such that the effect of the sarcolemma are not felt in the central region of the model. The attachment point of α -actinins to actin and the ends of actin are considered nodes (represented by red spheres) and the portions of actin filaments between nodes and the α -actinins are considered segments. All segments were modelled as Hookean springs with an elastic constant of 2280 pN/Å. No rotational constraints were applied to the segments at the nodes and all interconnected segments are linked via a node. Initially none of the nodes were subject to external forces and all segments measured zero tension. Since during an isometric contraction of a vertebrate striated muscle the tension per myosin filament in a half sarcomere rises to an estimated 480 pN (28), we assume here that such tension translates to 240 pN per actin filament in the half sarcomere's I band. For our first simulation, we applied a force to each outer node of the actin filaments. These forces were directed upwards for the nodes at the top of the model, and downwards for the nodes at the bottom (Fig S4 e). These forces had nominal value of 100 (corresponding to 100% of 240 pN) (Fig S4 c-e). The levels of tension calculated for the actin and α -actinin segments are shown in (e). While the actin filaments on both sides have tension of 100, the tension in the α -actinins is progressively less towards the centre of the Z-band (e) from 21 to 8. The lateral component of the tension is transmitted to the boundary of the whole region. To clarify what is done below, it is worth pointing out that the modelled region represented here corresponds to central region of the constructed model and that the tension values would be the same if the actin outer nodes at the bottom of the model were anchored i.e. kept fixed in space instead of having a force applied on them.

We next investigated the question of what is the effect of an actin filament having a different tension to its neighbours as could happen in a muscle during contraction. This is illustrated in the diagram of Fig S4f, corresponding to the central region of the full 3D model shown in Fig 4Sa,b. In this model the force applied to one of the actin outer nodes (marked with * in the diagram) is 10% bigger than the forces applied to the all the other actin outer nodes. Also, the actin outer nodes at the bottom of the model are anchored (this allows us to measure the changes in tension of the actin filaments, which would not be possible if a force was applied to the outer nodes and they were allowed to move). We found the 10% extra tension to be equally subdivided amongst the immediate neighbouring actins of the opposite side and very little beyond (compare the tension values in Fig S4e and S4f).

This simulation demonstrates the remarkable efficiency and small spatial extent of the shock absorber nature of the Z-band in smoothing out the variations that must occur in the tension produced by the myriads of myosin crossbridges acting on the actin filaments.

Discussion

While great progress has been made in understanding the molecular structures of the actin, myosin and their interaction in various states, little is known about the molecular structure of the sarcomeric skeleton like the Z-band and M-band. Understanding the molecular structure of the Z-band is important in order to understand how the tension generated during contraction is relayed by the Z-band from sarcomere to sarcomere along the myofibril. We have presented here the first molecular structure of the Z-band in vertebrate striated muscle, giving details of the conformation and interaction of actin and α -actinin. We have found that the Z-band crosslink is composed of α -actinin linking actin filaments mainly in the (11) plane and has an angle of 25° off the actin filament. The whole α -actinin link is quite straight with the ABD roughly following the path of the rod. Two important features of the rod have a distinct fit into the map. The slightly curved rod exactly matches the curvature of the link. Secondly the flattened slab-like profile of the rod matches the similar profile of the link in the map, giving edge-on views of the slab in transverse view and face view for the diagonal link in the (11) longitudinal view.

Comparison with previous Z-band 3D studies

Two previous 3D reconstructions of basketweave Z-bands have been reported (5, 29). Luther (29) investigated the structure of the Z-band in fish fin muscle, a fast muscle with a Z-band of width $\sim 700\text{\AA}$ and by modelling inferred that the number of α -actinin layers comprising it was three. Luther et al (5) studied bovine neck muscle, a slow muscle with a Z-band of width $\sim 1300\text{\AA}$ and also by modelling inferred that the number of layers was six. Because of the low resolution of the reconstructions, $\sim 100\text{\AA}$, no attempt was made to dock atomic models. The reconstructions look similar to the sonic Z-band obtained here.

Two small-square Z-band reconstructions have been reported. Morris et al (24) investigated the Z-band in nemaline rods found in skeletal muscle of humans with nemaline myopathy. Like the sonic muscle Z-band, nemaline rods comprise extended Z-band assemblies but in the small-square form. The reconstruction showed that the small-square Z-band did not have curved links but comprised links with right angle bends. Morris et al proposed that the four actin filaments within

each unit cell shown in Fig 1e were linked by two α -actinins with the rods located in the middle in close proximity and running parallel to the actin filaments. Burgoyne et al (30) studied the Z-band in rat cardiac muscle using dual axis tomography and subtomogram averaging. In both cases the resolution was not sufficient for atomic docking.

Suitability of sonic muscle to study Z-band structure

The sonic muscle Z-band is special because it is extraordinarily $\sim 1.2 \mu\text{m}$ wide in comparison with normal Z-bands which range from 70-150 nm. It exhibits the basketweave form homogeneously over the whole muscle. In comparison normal muscle myofibrils show the basketweave form or the small-square lattice form, but often both may be present in a single myofibril in various proportions (2). The sonic muscle Z-band is highly crystalline, hence it is ideal for structural analysis as it provides many easily identifiable subvolumes for input into subtomogram averaging.

The Z-band structure reported here pertains to the interior of the Z-band. Lacking in our analysis is structural information on the axially outermost links on each side of the Z-band (facing outward to the M-bands). Hence the Z-band structure reported here would be expected between, for example, link levels 2 to 5 in a 6-layer Z-band as found in slow and cardiac muscle (1). The axially outermost α -actinin link is predicted to be different as it may interact with titin (31). We note that while normal Z-bands have precisely defined widths (5, 6, 29, 32) with precisely defined edges, the outer edges of the sonic muscle Z-band appear quite ragged (Fig 1a), hence would not be suitable for determining outer-edge link structure.

Titin, the third most abundant protein in muscle, is $\sim 1 \mu\text{m}$ long and spans half sarcomeres from the M-band to the Z-band (33). It is responsible for maintaining the passive elasticity of muscle hence its tethering mechanism at both ends is important. In the Z-band, it is thought to bind to EF3-4 hands of α -actinin under the action of phospholipids which induce the open state of the ABD (11, 34, 35). **In the current modelling we have used the closed conformation of ABD due to the availability of its structure bound to actin by Galkin et al (26). At the current resolution it is difficult to distinguish between the open and closed conformations of ABD, so we cannot draw any effective conclusions on the ABD conformation. A future high resolution tomography study of a normal Z-band will be required to investigate how links between titin and α -actinin combine with the ABD-actin links to provide additional stability to the Z-band as demonstrated by Grison et al (34).**

Comparison of tomography of sonic muscle Z-band using transverse and longitudinal sections

For this study, the tomography analysis was done for both transverse (TS) and longitudinal (LS) sections. In each case, dual axis tomography was done followed by subtomogram averaging. The reconstruction from LS was not as informative as the TS, so it has not been described here. The reduced effectiveness of the LS tomogram is due to the differential shrinkage during exposure to the electron beam (20). Shrinkage is most pronounced along the tomogram z axis, and is often corrected by applying an appropriate stretch. For the LS tomogram, α -actinin links with different orientations will undergo differential shrinkage, and the results will be merged together during subtomogram averaging resulting in blurring and loss of resolution, which cannot be corrected by stretching. For the TS studies here, the dual axis tomogram revealed excellent detail into which molecular docking could be done. Since the TS and LS averages are not equivalent, combining the two datasets was not pursued.

Mechanical aspects of the Z-band

In this study we have established the geometry of the basketweave Z-band hence we can investigate how tension is handled in the Z-band. We set up a simple model to investigate the tensions in actin and α -actinin during contraction (Fig S4). For uniform tension in actins from adjoining sarcomeres, tension is progressively less towards the centre of the Z-band (Fig S4e). The interesting question is the effect of varying tension in the actins in the Z-band, a very likely effect of varying crossbridge activity. We investigated the effect by perturbing one actin by varying amounts (Fig S4f). We found this affects the immediate neighbouring actins of the opposite side and very little beyond. Our simulations demonstrate the shock absorber effect of the Z-band in smoothing out the variations that must occur in the tension produced by the myriads of myosin crossbridges acting on the actin filaments. The shock absorbing effect is much greater in the slow and cardiac muscles with up to 6 layers of α -actinin compared with the narrow Z-bands in fast-twitch muscles with 2 layers (data not shown). The contractile tension in the Z-band also has a transverse component. In striated muscle desmin intermediate filaments connect neighbouring myofibrils at the level of the Z-band. Mutations or deficit in desmin lead to skeletal or cardiac muscle disease (36) showing the importance of the transverse cytoskeletal network which the Z-band is part of.

Materials and Methods

Muscle preparation

Plainfin type I male midshipman fish were obtained off the coast of California, transported live and maintained in an artificial seawater aquarium at 15°C. Specimens were usually sacrificed soon after

arrival in the laboratory. Swim bladder muscle (sonic muscle) of the fish was dissected in fish Ringer (see below) with 50 mM BDM, 1mM DTT and Sigma cocktail 1:100 dilution. Fibre bundles $\sim 200 \mu\text{M}$, were dissected and mounted on plunge forks. They were skinned by immersion in relaxing solution with 0.5% Triton and 50 mM butanedione monoxime (BDM, 30 min). Single and a group of a few fibres were gently teased out. They were cryo-protected with 30% sucrose. The fibres were mounted on custom plunge-forks (37) and plunge frozen into liquid ethane using a Reichert KF80 plunge freeze machine. The fibres were freeze-substituted by immersing in acetone at -80°C for 3 days, then warmed up to -30°C , immersed into 1% osmium tetroxide in acetone at -30°C for 1 hour, warmed up to room temperature and fixed further for half hour, rinsed in acetone, immersed in 1:1 acetone/araldite overnight, into Araldite for 1 hour, then at 50°C for 30 min, new Araldite at 50°C for 30 min, then embedded in Araldite (2 days). Thin sections, $\sim 100\text{nm}$ thick, were cut with a Reichert Ultracut-E or RMC MT7 ultramicrotomes, coated with 100 \AA gold particles prepared by the method of (38) and stained with 2% uranyl acetate and Reynolds lead citrate. The electron microscopy was carried out using an FEI CM200 (Imperial College London), JEOL 1200 EX (Imperial College London) and FEI CM300-FEG (FSU, Tallahassee, FL).

Fish ringer in mM: NaCl, 186; KCl, 6.7; CaCl_2 , 3.8; MgCl_2 , 1.1; NaHCO_3 , 15; $\text{NaH}_2\text{PO}_4 \cdot \text{H}_2\text{O}$, 3. pH 7.4.

Fish Relaxing solution in mM: MgAcetate, 4; K_2EGTA , 5; Na_2ATP , 5; MOPS, 20; KMeSO_3 , 164, DTT, 1; Sigma Cocktail 1:100 diluted, ionic strength 230 mM, pH 7.0 at 20°C .

Electron microscopy

Dual axes tilt series were recorded with an FEI CM200 electron microscope using a Gatan 916 high tilt holder over the two ranges -62° to 70° and -70° to 70° in steps of 2° . The tilt series images were recorded using the automated procedure provided by Tietz EM-Menu software. The images were recorded at 27000x magnification on a Tietz FC415 camera with 4kx4k pixel resolution (www.tvips.com). The images were binned 2x and the final pixel size was 6.42 \AA . Tomography and combination of dual-axes tilt series were done using IMOD. The software PEET running under ETOMO was used for subtomogram averaging (21, 22). The Z-band subvolume marked by dashed outline box (Fig 1e) was defined as the “particle” for subtomogram averaging. Automatic particle picking was performed by iterative refinement starting from a manually chosen initial reference and a uniform 2D grid of initial locations with spacing approximating that of the unit cell. Selected points were windowed via cross-correlation thresholding and manual editing before further alignment and averaging

Acknowledgments

We thank Andrey Tsaturyan and William Lehman for helpful discussions. We thank John Wright of University of Texas at Austin for technical assistance. PKL was supported by BHF Programme Grant, RG/11/21/29335. KAT, JL and HW were supported by NIH grant GM30598. KW was supported by Intramural Research Program of NIAMS and by Taipei Medical University, Taiwan. Molecular graphics and analyses were performed with UCSF Chimera, developed by the Resource for Biocomputing, Visualization, and Informatics at the University of California, San Francisco, with support from NIH P41-GM103311.

Figure Legends

Figure 1.

The extraordinarily wide Z-band of midshipman fish and schematic drawings of relevant structures. (a-d) Electron micrographs of thin sections of swim bladder muscle of male Type 1 Plainfin midshipman fish. (a) Longitudinal section shows exceptionally wide (axially) $\sim 1.2 \mu\text{m}$ Z-bands with normal A-bands. (b-c) longitudinal sections of the Z-band showing clear lattice views; (b) (10) view, (c) (11) view. (d) Transverse section showing clear basketweave form. The lattice is ordered over $\sim 200 \text{ nm}$ clusters with clear dislocations between them. (e) The Z-band tetragonal lattice and nomenclature of lattice views. The main figure illustrates a slightly oblique lattice of actin filaments of one sarcomere (grey) at the left and actin filaments from an adjoining sarcomere at the right (red) and interdigitation of the filaments in the basketweave Z-band. Along the bottom, unit cells are outlined in the Z-band and on either side. Projecting about the major axes gives the lattice views we observe in longitudinal sections, like the (10) view with spacing 262 \AA and similar orthogonal (01) view. Projecting along the diagonal gives the (11) view with spacing 185 \AA . The dashed line box shows the size used for sub-volume averaging (discussed later). (f) An actin filament can be thought of as a 1-start, shallow helix in which the monomers are related by an axial rise of 27.4 \AA and a rotation of 167.1° so that every 7th actin subunit is spaced 192 \AA apart axially and rotated by 90° forming 4_3 screw symmetry. Binding sites for α -actinin are highlighted in red and blue to emphasize the screw symmetry of the paired binding sites. (g,h) α -actinin rod (Ylanne et al, 2001) fits into a rectangular slab of length 242 \AA , width 49 \AA (g) and depth 31 \AA (h). The slab face (g) comprises the 2-fold view (marked with central symbol) and the slab edge (h) shows the gently curved structure of the rod

Scale bars (a) = $1 \mu\text{m}$, (b,c,d) = 100 nm

Figure 2

Subtomogram average of the sonic muscle basketweave Z-band and fitting of atomic coordinates. Three columns are shown: Column (1), surface rendered views of subtomogram average; (2), docked atomic coordinates of actin and α -actinin and (3) only the atomic coordinates. Colour-coded axes are shown: x, red; y, green; z, blue. The first row (a-c) shows transverse view, 2nd row (d-f) shows longitudinal (11) view, 3rd row (g-i) shows (10) view, and 4th row (j-l) (01) view. The arrows on the actin filaments in (j & l) point towards the M-band; in the opposite direction is the actin barbed end (which resides in the Z-band).

Column 1 shows the clearest reconstruction of vertebrate muscle Z-band to date. It shows a unit cell of the Z-band (dashed box in (a)) composed of two pairs of actin filaments with opposite

orientation and a pair of α -actinins linking two antiparallel actins at a given axial level. Pairs of links separated axially by $\frac{1}{4}$ repeat (192 Å) are perpendicular to each other, yielding links to each actin filament in a rectangular motif (a). Column 2 shows the map with docked actins, two in yellow of one orientation and two in green of the opposite orientation. Added to actin coordinates are selected actin binding domains of α -actinin depicted in red. For clarity only two pairs of α -actinin rods are shown, in purple and blue. In transverse view (b) the arc of the rod matches nicely the gentle curve of the map link. Column 3 showing only the atomic coordinates demonstrates that the actin/ α -actinin assembly in the Z-band is sensible. The chevron motif (g) typical of longitudinal views is due to projection of multiple actins in the depth and is composed of two axially consecutive layers of α -actinin (purple and blue in (i)) giving an apparent repeat of 384 Å. This figure was prepared using Chimera (39). Scale is indicated in (a) for the transverse views by (11) lattice spacing of 185 Å and in (j) for longitudinal views by a vertical bar depicting 384 Å (half actin repeat).

Figure 3

Further scrutiny of the basketweave Z-band atomic structure using stereo views. To illustrate the orientation of the rods, they are enclosed in a slab of size 242x49x31 Å (also shown Fig 1g,h) (Ylanne et al, 2001). (a) Transverse view depicting a thin depth \sim 250 Å of the Z-band which includes a single α -actinin link with purple rod presenting slab edge-view. (b) Longitudinal (11) view depicting a thin depth of \sim 200 Å showing a diagonal α -actinin with purple rod in slab face-view making nearly straight links with ABDs. In this projection the orthogonal rods (blue) appear close to the actins, showing the origin of the dense actin filaments in electron microscope (11) views (Fig 1c). The arrows point to the M-band; the opposite direction is the actin barbed end (located in the Z-band). This figure was prepared using Chimera (39).

Supporting Information

Correction of ultramicrotomy compression of thin sections

To enable accurate subtomogram averaging and symmetrisation over particles with varying orientations, it is essential that the sample not be distorted. Our correction of section compression typical of thin sections prepared by ultramicrotomy is discussed here. Our sample, which consists of sections of resin-embedded tissue prepared by ultramicrotomy, suffered from compression along the cutting direction. The direction (but not the amount) of compression can sometimes be seen in sections by scores in the section due to imperfections in the diamond or glass knife cutting edge. For transverse sections of striated muscle we are fortunate that our prior knowledge that the lattice is square allows us to determine the direction and the amount of the compression (Fig S1). The Fourier transform (FT) (Fig S1b) of the outlined cluster in Fig S1a comprises discrete spots lying on a parallelogram rather than on a square expected from a tetragonal lattice. As the various clusters occupying the two myofibrils in Fig S1a have different orientations, the FT of the whole image gives spots lying on different locations on an ellipse (Fig S1c). We used least-squares fitting to determine the parameters of the ellipse. These parameters specify the distortion of the lattice: the longer reciprocal axis gives the direction of the compression and the ratio of the shorter to the longer axes gives the amount of compression. Then the tomogram was stretched in the appropriate direction and amount and the result is shown in Fig S1d. The FT of the corrected cluster gives spots lying on a square lattice (Fig S1e) and the FT of the whole image gives spots lying on concentric circles (Fig S1f).

Scaling of dimensions in map

Plastic embedded samples typically shrink during chemical processing and embedding. Additional shrinkage occurs during electron microscopy due to the electron radiation (20). It is necessary to correct for this shrinkage prior to the fitting of the atomic structures. The shrinkage in the depth (z) has to be considered separately from the shrinkage in the plane of the section. For the transverse sections used here, the z-scale was obtained by comparing features of the actin and immediate link density in the map with features from the atomic model of the actin-ABD composite (described in the next section). By examining the full averaged map (Fig S3b and Movie S2), we can estimate that the depth of the native sample encloses 3 half-repeats of actin (384 Å). Half-repeats of 384 Å along the axis can be identified in Fig S3b by neighbouring arrowhead motifs along actin.

In the plane of the section (i.e. for the Z-band lattice), the Z-band structure has been scaled relative to the A-band lattice in fish muscle determined by X-ray diffraction of fish muscle which has

a value of 472 Å inter-myosin filament spacing (40). Next we used an electron micrograph of a longitudinal section of the sonic muscle that showed complete sarcomeres and selected those that showed clear lattice views for both the A-band and the Z-band. Assuming that any dimension change would affect the A-band and Z-band equally, we used simple geometry to scale the micrograph and determined that the Z-band lattice has a spacing of 262 Å.

Figure S1

Correction of microtome compression of the section. (a) Projection of the tomogram of sonic muscle Z-band showing clear basketweave form. The two myofibrils are composed of ordered lattice clusters with varying orientations like the one outlined. The clusters can be seen by viewing the image at a glancing angle. The black line running approximately parallel to the y-axis represents the direction of compression. (b,b') FT of the outlined domain in (a) shows discrete Fourier spots lying on parallelograms. The (11) Fourier spot at 1/185 Å spacing is shown. (c,c') FT of the whole image (a) produces Fourier spots scattered along elliptical paths, with the major and minor axes marked (a,b). (d) Result of stretching the tomogram along the black line in (a) parallel to the direction of the major ellipse axis a in (c'). (e,e') The FT spots of the corrected Z-band in the outlined cluster now lie on square lattices. (f,f') The FT of the whole corrected image (d) produces spots lying along concentric circles. Scale bar in (a,d) = 100 nm

Figure S2

The resolution of the subtomogram average estimated by the Fourier Shell Correlation using a threshold of 0.5 is 39 Å. This is a good resolution for a plastic embedded sample. See text for further discussion.

Figure S3

Projection images of the subtomogram average computationally cloned back into original volume. This is also shown in Movie S3. (a) Projection of tomogram to give transverse view showing the basketweave form. Close inspection shows the dislocations between the different domains with varying orientations. (b & c) Longitudinal projections perpendicular to black line in (a). (b) Fine ~50 Å projection showing clear arrowhead motif of ABDs every ½ actin repeat (384 Å). (c) Thicker projection ~100 nm, comparable to view in common thin sections, showing the chevron appearance typical of vertebrate muscle Z-bands (cf Fig 1b). Scale bar in a,b,c = 100 nm.

Figure S4

Simulations of tension handling in the Z-band. (a,b) A simple model of the Z-band was set up comprising a circular area of diameter $\sim 0.5 \mu\text{m}$. Lattice size was 262 \AA . The α -actinin link was modelled as a straight link connecting the actin filaments at the ABD attachment positions. Four layers of links with axial separation of 192 \AA with relative rotation of 90° were modelled. The link ends represent nodes (shown in red circles). (c,d) Close-up of small central region of the model overlaid with Z-band average in (10) view. (d) Stereo-view of model. (e) Tension values in the Z-band for equal nominal force of 100 applied to the actin outer nodes on both sides. Tension in actin reduces through the Z-band towards the actin barbed end and tension in α -actinin reduces towards the centre of the Z-band. (f) Effect of perturbation of 10% on one actin filament (marked with *). In this case the actin filament ends in bottom sarcomere are anchored. The tension reduces to 102 in the immediate neighbouring anti-parallel actins, hence the tension is dissipated quickly across the Z-band, illustrating the shock absorber nature of the Z-band architecture.

Movie S1

Movie of the raw tomogram of sonic muscle Z-band paging through a full cycle of the stack starting from the centre. In this $\sim 100 \text{ nm}$ thick section, the basketweave motif cycles in and out of view a few times in the stack transit. 10 nm gold particles are present at the surface.

Movie S2

Movie of "cloned" tomogram paging through stack. Comparable to Movie S1-M1 but with the subtomogram average inserted at each particle point in the original tomogram with appropriate orientations as determined during subtomogram alignment and averaging. The Z-band basketweave structure is very clear as are the dislocations between the Z-band domains.

Movie S3

Movie of subtomogram average and fitting into map of actin and α -actinin. This is the first detailed view of vertebrate muscle Z-band in the basketweave state. The movie comprises three parts: the Z-band average alone, then with fitted actin and α -actinin rod coordinates, and finally just actin and α -actinin rod coordinates alone. Two actins of one orientation are shown in green and two are shown in yellow. The coordinates for actin binding domain of α -actinin were first docked into the actin coordinates found in previous studies(26) (red). For clarity only two pairs of α -actinin rods are

shown (blue and purple). At the resolution achieved (39Å), the fit of the coordinates is excellent. The gentle curve of the rod fits nicely with the observed basketweave structure.

References

1. Luther PK (2009) The vertebrate muscle Z-disc: sarcomere anchor for structure and signalling. *J Muscle Res Cell Motil* 30(5-6):171-185.
2. Perz-Edwards RJ & Reedy MK (2011) Electron microscopy and x-ray diffraction evidence for two z-band structural States. *Biophys J* 101(3):709-717.
3. Goldstein MA, Michael LH, Schroeter JP, & Sass RL (1988) Structural states in the Z band of skeletal muscle correlate with states of active and passive tension. *J. Gen. Physiol.* 92(1):113-119.
4. Luther PK (1995) Symmetry of a vertebrate muscle basketweave Z-Band. *Journal of Structural Biology* 115(3):275-282.
5. Luther PK, Barry JS, & Squire JM (2002) The three-dimensional structure of a vertebrate wide (slow muscle) Z-band: lessons on Z-band assembly. *J Mol Biol* 315(1):9-20.
6. Luther PK, Padron R, Ritter S, Craig R, & Squire JM (2003) Heterogeneity of Z-band structure within a single muscle sarcomere: implications for sarcomere assembly. *J Mol Biol* 332(1):161-169.
7. Frank D, Kuhn C, Katus HA, & Frey N (2006) The sarcomeric Z-disc: a nodal point in signalling and disease. *J Mol Med* 84(6):446-468.
8. Otey CA & Carpen O (2004) Alpha-actinin revisited: a fresh look at an old player. *Cell Motil Cytoskeleton* 58(2):104-111.
9. Sjoblom B, Salmazo A, & Djinovic-Carugo K (2008) Alpha-actinin structure and regulation. *Cell Mol Life Sci* 65(17):2688-2701.
10. Blanchard A, Ohanian V, & Critchley D (1989) The structure and function of alpha-actinin. *J. Muscle Res. Cell Motil.* 10(4):280-289.
11. Ribeiro Ede A, Jr., *et al.* (2014) The Structure and Regulation of Human Muscle alpha-Actinin. *Cell* 159(6):1447-1460.
12. Hampton CM, Taylor DW, & Taylor KA (2007) Novel structures for alpha-actinin:F-actin interactions and their implications for actin-membrane attachment and tension sensing in the cytoskeleton. *J Mol Biol* 368(1):92-104.
13. Ylanne J, Scheffzek K, Young P, & Saraste M (2001) Crystal structure of the alpha-actinin rod reveals an extensive torsional twist. *Structure (Camb)* 9(7):597-604.
14. Luther PK, *et al.* (2008) Understanding the organisation and role of myosin binding protein C in normal striated muscle by comparison with MyBP-C knockout cardiac muscle. *J Mol Biol* 384(1):60-72.
15. Lewis MK, *et al.* (2003) Concentric intermediate filament lattice links to specialized Z-band junctional complexes in sonic muscle fibers of the type I male midshipman fish. *J Struct Biol* 143(1):56-71.
16. Bass AH & Marchaterre MA (1989) Sound-generating (sonic) motor system in a teleost fish (*Porichthys notatus*): sexual polymorphism in the ultrastructure of myofibrils. *J Comp Neurol* 286(2):141-153.
17. Ostap EM (2002) 2,3-Butanedione monoxime (BDM) as a myosin inhibitor. *J Muscle Res Cell Motil* 23(4):305-308.

18. Amos LA, Henderson R, & Unwin PN (1982) Three-dimensional structure determination by electron microscopy of two-dimensional crystals. *Prog. Biophys. Mol. Biol.* 39(3):183-231.
19. Luther PK & Crowther RA (1984) Three-dimensional reconstruction from tilted sections of fish muscle M- band. *Nature* 307(5951):566-568.
20. Luther PK (2006) Sample shrinkage and radiation damage of plastic sections. *Electron Tomography: Methods for three-dimensional visualization of structure in the cell*, ed Frank J (Springer), pp 17-40.
21. Heumann JM, Hoenger A, & Mastrorade DN (2011) Clustering and variance maps for cryo-electron tomography using wedge-masked differences. *J Struct Biol* 175(3):288-299.
22. Nicastro D, *et al.* (2006) The molecular architecture of axonemes revealed by cryoelectron tomography. *Science* 313(5789):944-948.
23. Miller A & Tregear RT (1972) Structure of insect fibrillar flight muscle in the presence and absence of ATP. *J Mol Biol* 70(1):85-104.
24. Morris EP, Nneji G, & Squire JM (1990) The three-dimensional structure of the nemaline rod Z-band. *J Cell Biol* 111(6 Pt 2):2961-2978.
25. Luther PK & Squire JM (2002) Muscle Z-band ultrastructure: titin Z-repeats and Z-band periodicities do not match. *J Mol Biol* 319(5):1157-1164.
26. Galkin VE, Orlova A, Salmazo A, Djinojic-Carugo K, & Egelman EH (2010) Opening of tandem calponin homology domains regulates their affinity for F-actin. *Nat Struct Mol Biol* 17(5):614-616.
27. Holmes KC, Popp D, Gebhard W, & Kabsch W (1990) Atomic model of the actin filament. *Nature* 347(6288):44-49.
28. Piazzesi G, *et al.* (2007) Skeletal muscle performance determined by modulation of number of Myosin motors rather than motor force or stroke size. *Cell* 131(4):784-795.
29. Luther PK (2000) Three-dimensional structure of a vertebrate muscle Z-band: implications for titin and alpha-actinin binding. *J Struct Biol* 129(1):1-16.
30. Burgoyne T, Morris EP, & Luther PK (2015) Three-Dimensional Structure of Vertebrate Muscle Z-Band: The Small-Square Lattice Z-Band in Rat Cardiac Muscle. *J Mol Biol* 427(22):3527-3537.
31. Young P, Ferguson C, Banuelos S, & Gautel M (1998) Molecular structure of the sarcomeric Z-disk: two types of titin interactions lead to an asymmetrical sorting of alpha-actinin. *Embo J.* 17(6):1614-1624.
32. Luther PK (1991) Three-dimensional reconstruction of a simple Z-band in fish muscle. *J Cell Biol* 113(5):1043-1055.
33. Granzier H & Labeit S (2007) Structure-function relations of the giant elastic protein titin in striated and smooth muscle cells. *Muscle Nerve* 36(6):740-755.
34. Grison M, Merkel U, Kostan J, Djinojic-Carugo K, & Rief M (2017) alpha-Actinin/titin interaction: A dynamic and mechanically stable cluster of bonds in the muscle Z-disk. *Proc Natl Acad Sci U S A* 114(5):1015-1020.
35. Young P & Gautel M (2000) The interaction of titin and alpha-actinin is controlled by a phospholipid-regulated intramolecular pseudoligand mechanism. *EMBO J* 19(23):6331-6340.
36. Capetanaki Y, Papathanasiou S, Diokmetzidou A, Vatsellas G, & Tsikitis M (2015) Desmin related disease: a matter of cell survival failure. *Curr Opin Cell Biol* 32:113-120.
37. Cantino ME, Brown LD, Chew M, Luther PK, & Squire JM (2000) A-band architecture in vertebrate skeletal muscle: polarity of the myosin head array. *J Muscle Res Cell Motil* 21(7):681-690.
38. Slot JW & Geuze HJ (1985) A new method of preparing gold probes for multiple-labeling cytochemistry. *Eur J Cell Biol* 38(1):87-93.
39. Pettersen EF, *et al.* (2004) UCSF Chimera--a visualization system for exploratory research and analysis. *J Comput Chem* 25(13):1605-1612.

40. Harford J & Squire J (1986) "Crystalline" myosin cross-bridge array in relaxed bony fish muscle. Low-angle x-ray diffraction from plaice fin muscle and its interpretation. *Biophys J* 50(1):145-155.

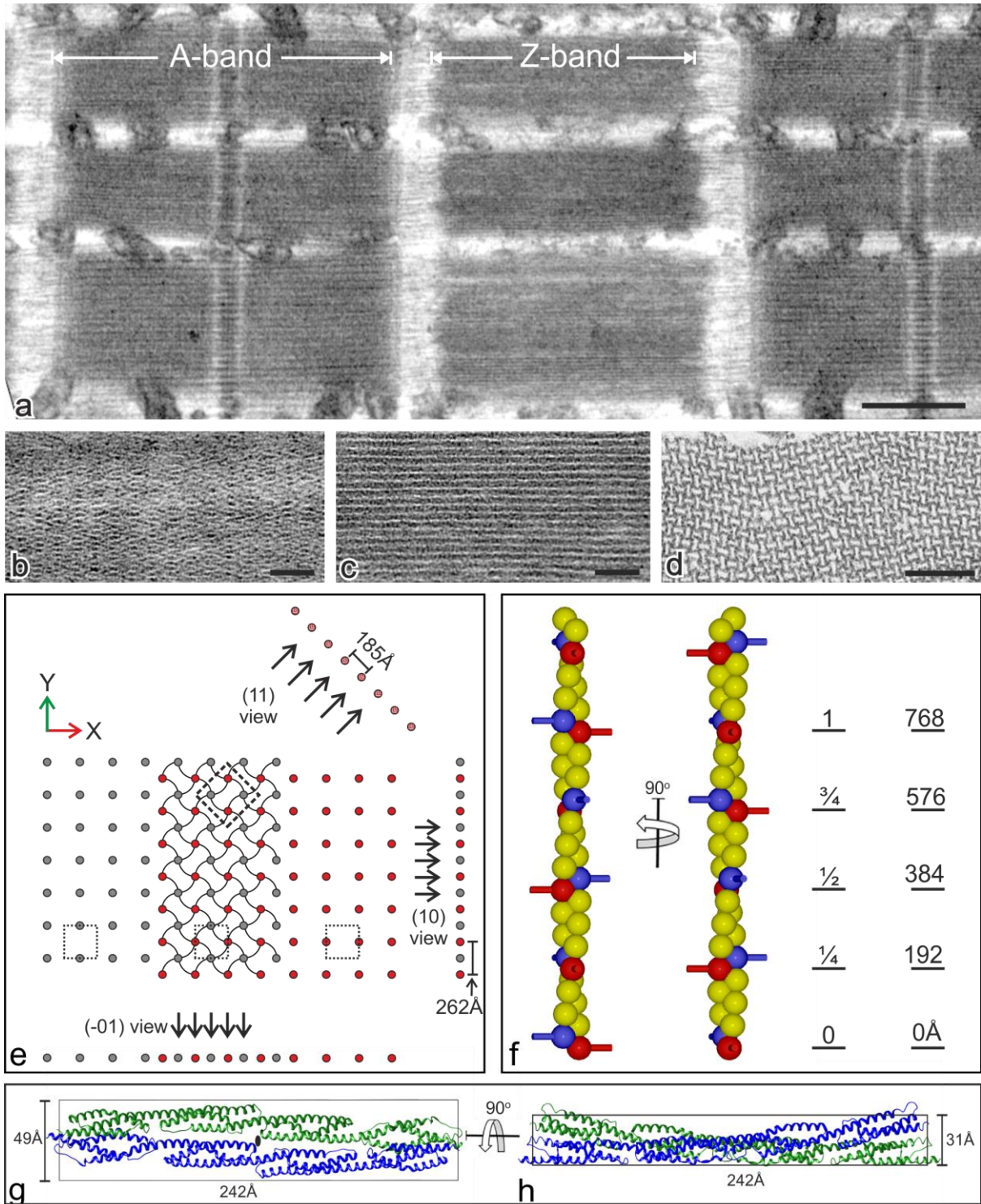


Figure 1

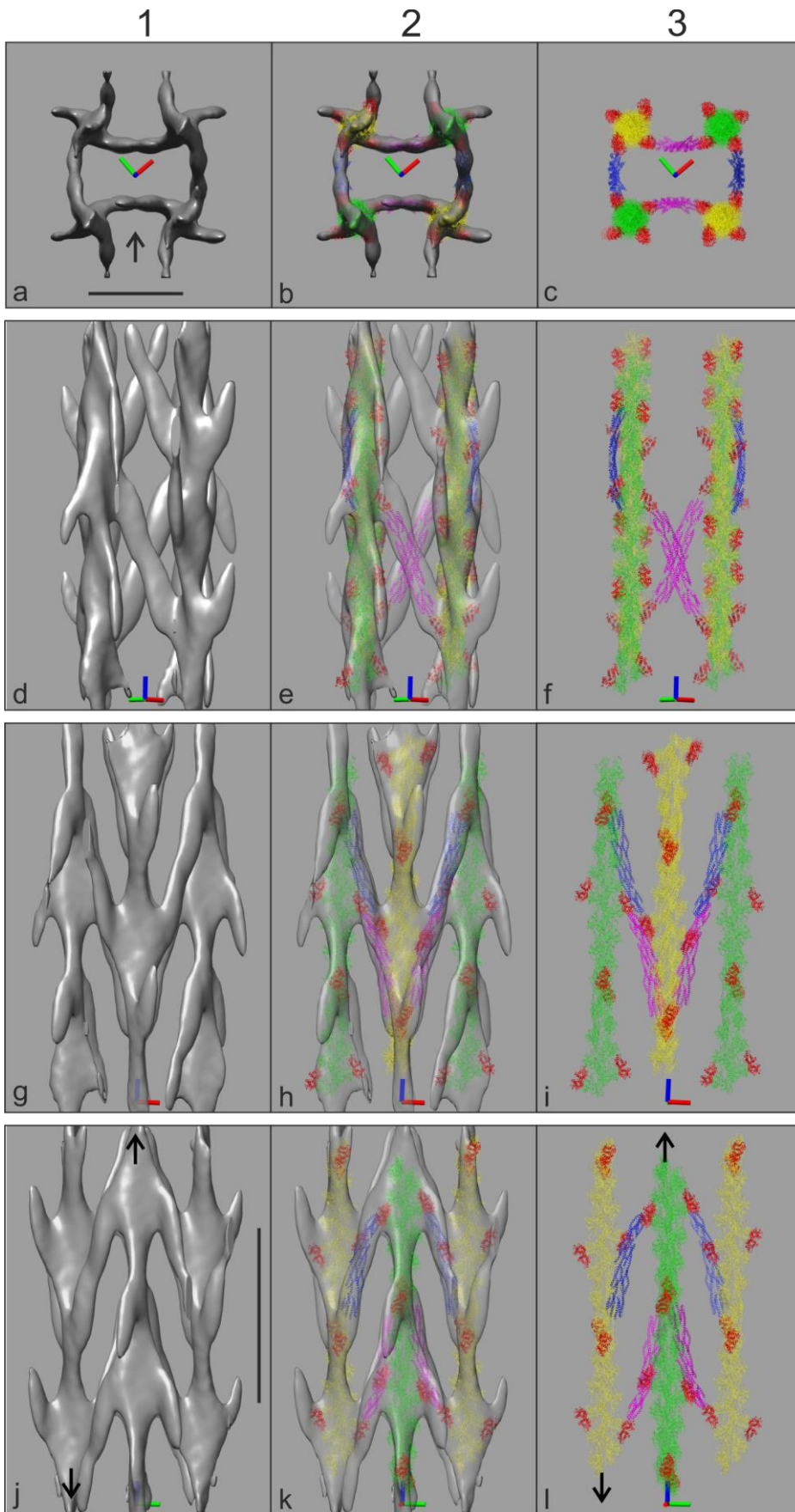


Figure 2

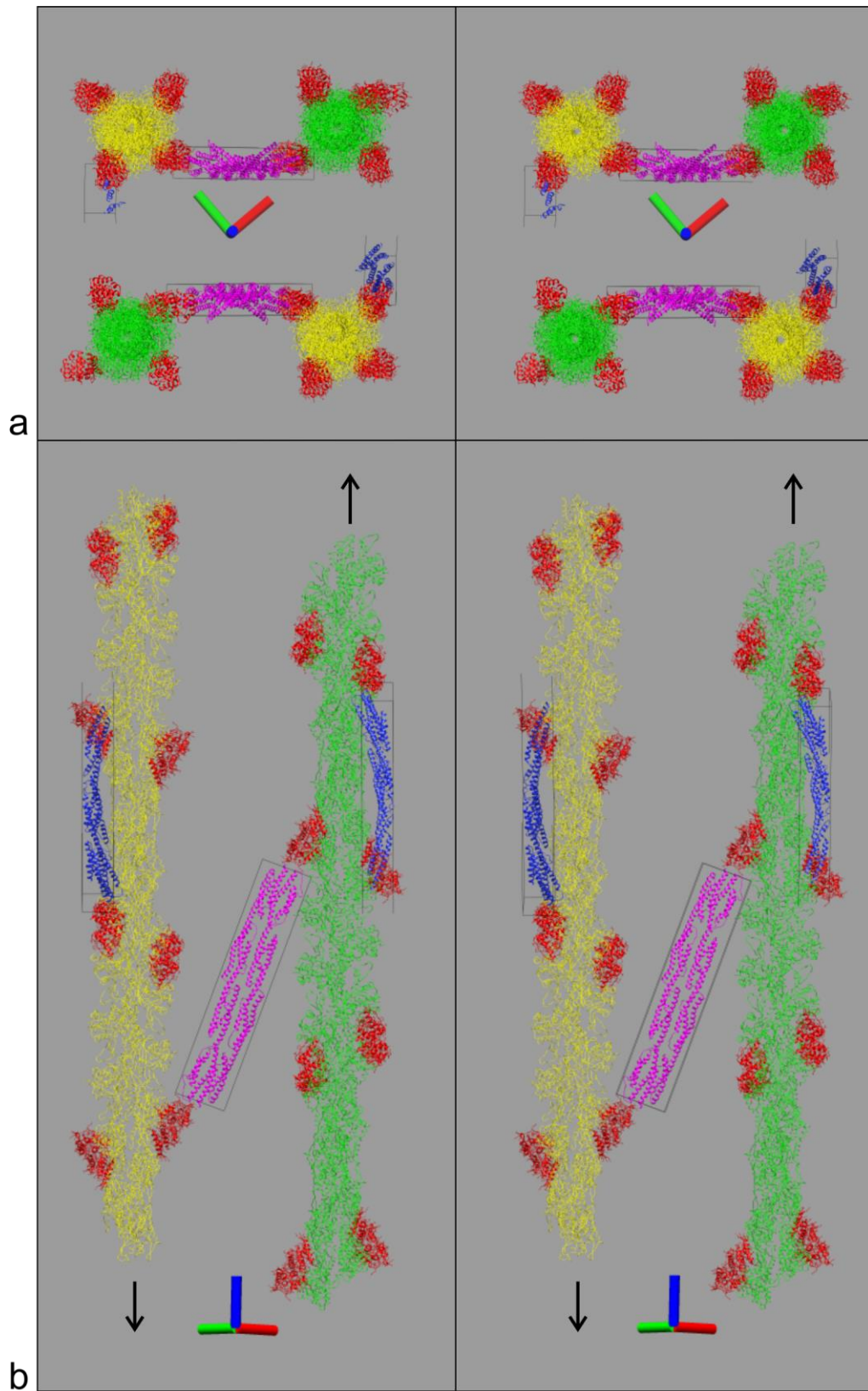


Figure 3